Journal of Materials and Construction
ISSN 2734-9438
Website: www. jomc.vn

Evaluation of the strength, dimensional stability, and microstructure of lightweight alkali-activated mortar incorporating used coffee grounds

Nguyen Van Dung[1], Ngo Si Huy[1], Huynh Trong Phuoc[2,*]

[1] Faculty of Engineering, Technology, and Communication, Hong Duc University

[2] Faculty of Civil Engineering, College of Engineering, Can Tho University

KEYWORDS

Compressive strength
Drying shrinkage
Lightweight composite
Microstructure
Segregation

ABSTRACT

Due to the shortage of natural river sand and the uncontrolled disposal of coffee waste, this study investigates the use of used coffee grounds (UCG) as a partial replacement for fine aggregate in producing lightweight alkali-activated mortar (LAAM). Coal bottom ash (BA) was replaced with UCG at 0%, 5%, 10%, and 15% by volume. Experimental evaluations included segregation resistance, compressive strength, ultrasonic pulse velocity (UPV), drying shrinkage, and microstructural analysis. The results showed that all mixtures exhibited acceptable homogeneity without significant segregation. A 5% UCG replacement increased compressive strength and UPV compared with the control mixture, owing to improved matrix compactness and internal curing. However, higher UCG contents led to reduced compressive strength and UPV values. Drying shrinkage decreased in UCG-modified mixtures, with LC-15 exhibiting the lowest shrinkage (best dimensional stability). SEM observations confirmed denser gel formation and better particle matrix bonding in LC-05, whereas LC-10 and LC-15 showed weaker interfaces and more voids. A 5% UCG content is recommended for practical application. These findings highlight the potential of UCG as an environmentally friendly alternative to fine aggregate for lightweight composites, supporting waste valorization and reducing the consumption of natural sand.

1. Introduction

The accelerating expansion of the construction sector has intensified the demand for natural resources, particularly fine aggregates such as river sand. This surge in consumption has contributed to the depletion of natural sand deposits and serious ecological disruption in river systems. In Vietnam, for instance, the Ministry of Construction has reported that the demand for construction sand has already surpassed the supply capacity of existing river sand reserves [1]. Meanwhile, global coffee consumption continues to rise, leading to the generation of millions of tons of used coffee grounds (UCG) each year. As stated in a previous study [2], more than six million tons of UCG are generated annually, and a considerable proportion remains unused. When disposed of in landfills, UCG undergoes biodegradation, releasing methane, carbon dioxide, and other greenhouse gases that contribute to climate change [2]. Consequently, converting this abundant organic waste into construction materials is consistent with sustainable development trends and circular economy strategies [3].

A variety of studies have confirmed the feasibility of incorporating UCG into different construction materials, including ceramics [4], lightweight aggregates [5], alkali-activated bricks [6], and cementitious composites [7]. Eliche-Quesada et al. [8] incorporated UCG into clay bricks, reporting a reduced density and enhanced thermal insulation. Likewise, Andreola et al. [5] demonstrated that UCG-based lightweight clay aggregates could increase porosity without significantly compromising strength. Lachheb et al. [9] found that the inclusion of UCG in cement-based composites improved thermal insulation due to the porous, organic nature of the particles. Collectively, these results suggest that UCG has potential as a lightweight filler that enhances the physical and functional properties of construction materials.

Research on cement-based systems has also shown promising mechanical and durability performance when UCG is used to partially replace natural sand. Roychand et al. [10] reported that thermally treated UCG can enhance concrete compressive strength by as much as 30 % when added in optimized proportions. Na et al. [7] observed improved microstructural quality and hydration behavior in mortars containing activated carbon derived from UCG. In addition, Lee et al. [11] confirmed that low-level UCG substitution could maintain acceptable strength and reduce density, although excessive replacement may result in strength loss due to poor interfacial bonding and increased porosity [12]. Beyond mechanical performance, UCG incorporation has been shown to enhance thermal and acoustic properties. Yun et al. [13] demonstrated that UCG can be repurposed into sound-absorbing panels, while Lachheb et al. [9] observed significant improvements in thermal resistance. Moussa et al. [14] further suggested that UCG-based composites are well-suited for

*Corresponding author: htphuoc@ctu.edu.vn
Received 09/01/2026, revised 25/02/2026, accepted 11/05/2026
Link DOI: https://doi.org/10.54772/jomc.v16i01.1219

non-load-bearing applications, supporting sustainable construction and indoor comfort.

Although numerous alternative materials have been explored as sand substitutes in alkali-activated mortars/ composites, the incorporation of UCG remains relatively underdeveloped and insufficiently understood. Lightweight alkali-activated materials (AAMs) have recently received increasing attention due to their potential to reduce density while maintaining acceptable mechanical performance and sustainability advantages. In alkali-activated slag (AAS) mortars, the incorporation of lightweight fine aggregates has been shown to influence pore structure evolution and matrix continuity, thereby affecting durability-related phenomena such as efflorescence and moisture transport [15]. Furthermore, studies on geopolymer mortars incorporating lightweight aggregates have demonstrated that aggregate absorption capacity and pre-conditioning strongly influence fresh-state stability and hardened microstructure development [16]. These findings highlight that the performance of lightweight AAM systems is highly sensitive to aggregate porosity, moisture exchange, and interfacial characteristics – factors directly relevant to the present BA–UCG system. In particular, limited studies have systematically examined the combined effects of UCG incorporation on segregation resistance, compressive strength, ultrasonic pulse velocity, drying shrinkage, and microstructural characteristics within fly ash–ground granulated blast furnace slag–based lightweight alkali-activated mortar (LAAM). The present study is therefore positioned as a mechanistically interpreted performance investigation rather than a chemically resolved reaction analysis. The emphasis is placed on establishing a continuity-controlled framework that links UCG morphology, pore connectivity, interfacial transition zone (ITZ) characteristics, and matrix compactness to the coupled evolution of compressive strength, UPV, and drying shrinkage in FA–GGBFS LAAM. While previous studies have reported strength variations in UCG- or bio-waste-modified geopolymer systems [10], [11], a systematic segregation–UPV–shrinkage–SEM coupling analysis within this specific binder system remains limited. Moreover, the underlying trade-off between the internal curing potential of highly porous UCG particles and the associated increase in matrix porosity and interfacial weakness has not yet been clearly clarified. Internal curing is moisture release from pre-wetted porous reservoirs that mitigates self-desiccation and reduces shrinkage-driving capillary stresses, while potentially improving microstructural development. In AAM systems, recent work has further demonstrated that internal curing agents/porous aggregates can mitigate autogenous shrinkage of AAS mortars and improve volumetric stability, although excessive porous inclusion may increase connected voids and reduce mechanical stiffness. This dual influence provides a relevant conceptual basis for interpreting the competing effects of UCG as a highly absorptive porous filler in FA–GGBFS matrices [17], [18]. To address these deficiencies, the present study evaluates the strength, dimensional stability (drying shrinkage), structural integrity indicators (UPV), and microstructural characteristics of LAAM incorporating UCG at replacement levels of 0 %, 5 %, 10 %, and 15 %. The findings are expected to advance sustainable construction practices by converting coffee waste into a valuable engineering material while reducing dependence on natural sand and mitigating environmental pollution.

2. Materials and experimental methods

2.1. Materials and mixture proportions

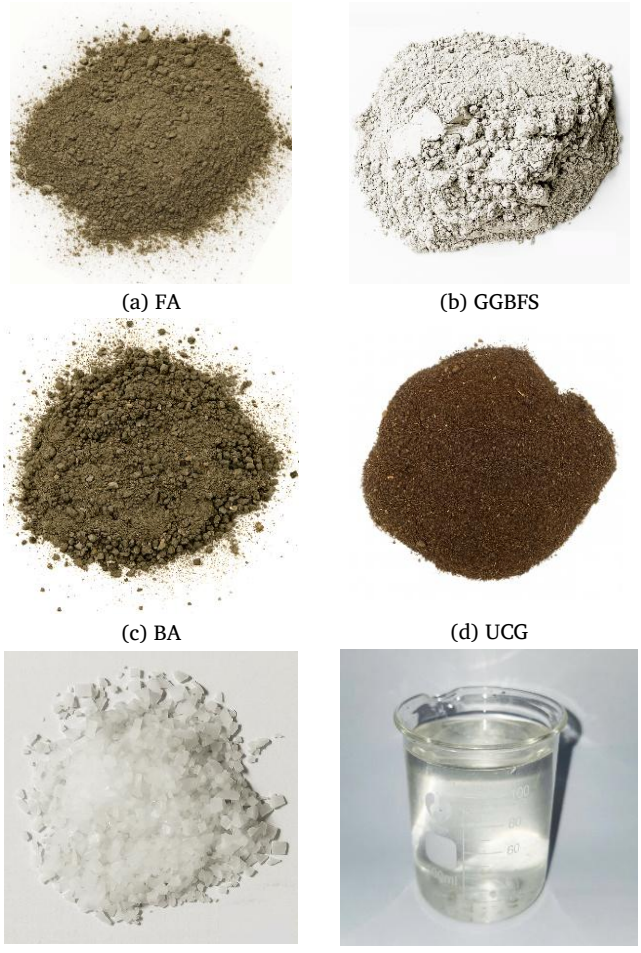

(a) FA (b) GGBFS (c) BA (d) UCG (e) SH (f) SS

Figure 1. Raw materials used for making LAAM.

Fly ash (FA) and ground granulated blast-furnace slag (GGBFS) were used as the primary binder materials to produce the LAAM in this study. The major chemical components of FA were SiO_2 (50.3 %), Al_2O_3 (35.6 %), Fe_2O_3 (5.2 %), and CaO (1.2 %), whereas GGBFS mainly consisted of SiO_2 (33.9 %), Al_2O_3 (14.4 %), CaO (40.8 %), and MgO (6.7 %). Their specific gravities were 2.27 and 2.85, respectively. Both FA and GGBFS contain substantial quantities of SiO_2, Al_2O_3, and CaO, which are known to play crucial roles in the polymerization process of alkali-activated materials. The alkaline activator used for the LAAM was a mixture of sodium hydroxide (SH) and sodium silicate (SS) solutions. The SH solution was prepared at a

concentration of 5 M, with a density of 1.19 g/cm^3, while the SS solution had a density of 1.38 g/cm^3. The SS-to-SH ratio was selected based on the required alkali modulus (Ms, the molar ratio of SiO_2/Na_2O) and alkali equivalent (AE, Na_2O content relative to binder mass) to ensure consistent reactivity across all mixtures. The SS solution used in this study had a SiO_2 content of 25.7 %, Na_2O content of 8.6 %, and water content of 65.7 %, corresponding to a silica modulus (SiO_2/Na_2O) of approximately 2.99. The mass ratio of SS to SH solution was maintained at 0.62 for all mixtures. The overall Ms of the activator system was fixed at 0.8, and the AE was controlled at 5 %. These parameters were kept constant to ensure comparable reaction kinetics and gel formation across all LAAM mixtures.

The fine aggregate system consisted of coal bottom ash (BA) and UCG. The BA, characterized by a fineness modulus (FM) of 2.42, water absorption of 8.2 %, and a particle density of 2.15 g/cm^3, served as the reference lightweight aggregate. In contrast, UCG exhibited an FM of 2.24, significantly higher water absorption of 88.7 %, and a lower density of 1.25 g/cm^3. Local tap water was used during the mixing process, and the natural appearances of all raw materials are shown in Figure 1.

Before mixing, both aggregates were conditioned to a saturated surface-dry state to ensure consistent water content and to prevent excessive absorption during blending. Due to the extremely high water absorption of UCG, the particles were pre-soaked in water and subsequently drained and surface-dried using absorbent paper until no visible free water remained. To enable complete internal pore saturation, the UCG particles were pre-soaked in drinkable water for 24 hours. After soaking, the extra water was sieved off until there was no more visible surface water. By making sure there was no free water buildup during weighing and no moisture transfer onto dry filter paper upon contact, the saturated surface-dry (SSD) condition was confirmed. This process was used to keep the liquid-to-solid ratio constant and reduce uncontrolled water absorption during mixing. The mixing water content was strictly controlled according to the designed liquid-to-solid ratio, and no additional water was introduced during mixing to compensate for UCG absorption. This procedure was adopted to maintain mixture consistency and ensure repeatability among all test batches. The incorporation of UCG as a partial replacement for BA was expected to reduce composite density and enhance sustainability by utilizing an organic waste material.

All LAAM mixtures were designed in accordance with the mix-design procedure described by Nguyen et al. [19]. The binder system employed a fixed FA/GGBFS mass ratio of 30:70, which has been reported to provide optimal strength and setting behavior for blended alkali-activated materials. A constant alkali equivalent of 5 %, an alkali modulus of 0.8, and a liquid-to-solid ratio of 0.42 were applied across all mixtures to ensure comparable reaction kinetics and workability. To evaluate the influence of UCG incorporation, BA was partially replaced with UCG at 0 %, 5 %, 10 %, and 15 % by volume. The detailed mixture proportions are presented in Table 1.

Table 1. Material proportions for 1 m^3 LAAM.

Mixtures	LC-00	LC-05	LC-10	LC-15
FA (kg)	187	187	187	187
GGBFS (kg)	436	436	436	436
SH (kg)	151	151	151	151
SS (kg)	94	94	94	94
BA (kg)	934	888	841	794
UCG (kg)	0	27	54	82
Water (kg)	136	136	136	136

2.2. Sample preparation and test methods

The preparation of LAAM specimens was carried out through four sequential stages to ensure consistency and reproducibility. In the first stage, all raw materials, including binders, aggregates, and activator components, were prepared according to the mixture proportions summarized in Table 1. The alkaline activator was produced by blending sodium hydroxide and sodium silicate solutions at the predetermined ratio until a clear and homogeneous solution was obtained. The activator was prepared at least 24 hours before mixing to allow temperature stabilization and ensure complete dissolution of sodium hydroxide pellets. In the second stage, the dry binders (FA and GGBFS) were placed in a laboratory pan mixer and blended for 2 minutes to achieve uniform dispersion. The prepared activator solution was then gradually added while mixing continued, followed by an additional 3 minutes of mixing to obtain a homogeneous alkali-activated paste. In the third stage, the BA and UCG aggregates were incorporated into the paste, followed by minor adjustment of workability within the limits of the designed liquid-to-solid ratio. Mixing continued until a uniform and cohesive consistency was achieved, ensuring even distribution of aggregates without segregation or lump formation. Workability was evaluated using a flow table test in accordance with ASTM C1437-20 [20]. The flow diameter of the mixtures ranged between 210 and 220 mm, indicating comparable consistency among all mixtures. No significant bleeding or segregation was observed during the flow assessment. Finally, in the fourth stage, the fresh LAAM mixture was cast into molds of various dimensions depending on the specific testing requirements. After 24 hours, the specimens were demolded and subsequently air-cured in an indoor laboratory environment at a temperature of 27 ± 2 ˚C and relative humidity of 65 ± 5 %. The specimens were stored under unsealed conditions to simulate practical exposure environments. No additional thermal curing or moisture sealing was applied. Compressive strength and UPV were evaluated at 7, 28, and 56 days, while drying shrinkage measurements were conducted up to 56 days.

The segregation potential test was conducted 1 day after casting, following the procedure described by Thang et al. [21]. Segregation is a known challenge for lightweight mixtures due to the density contrast between constituents, and quantitative assessment is

commonly performed by evaluating aggregate distribution through section-based density variation and/or image analysis of cross-sections. Such approaches have been widely used to characterize segregation in lightweight aggregate concretes and to compare mixture stability when lightweight constituents are incorporated [22], [23]. A cylindrical specimen with a diameter of 10 cm and a height of 20 cm was cut into five equal sections as illustrated in Figure 2. The bulk density of each section was measured and compared with the average value to evaluate the variation. The compressive strength of the LAAM mixtures was tested in accordance with ASTM C349-18 [24] using portions of prisms (4 × 4 × 16 cm) broken in flexure. Tests were performed at 7, 28, and 56 days. Ultrasonic pulse velocity (UPV) measurements were conducted on cylindrical specimens (10 cm in diameter and 20 cm in height) following ASTM C597-22 [25] at 7, 28, and 56 days. Drying shrinkage was measured on prismatic samples (2.5 × 2.5 × 28.5 cm) according to ASTM C490/C490M-21 [26] at 3, 7, 28, and 56 days. All compressive strength, UPV, and drying shrinkage results presented in this study represent the average of at least three measurements. After the compressive strength tests, small fragments of the broken specimens were collected for microstructural examination using scanning electron microscopy (SEM).

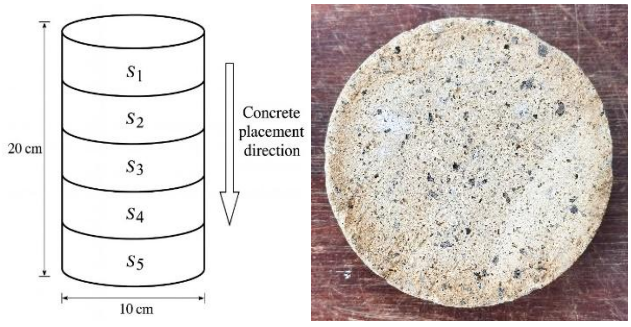

Figure 2. Specimen division diagram for determining segregation of LAAM.

3. Results and discussion

3.1. Segregation possibility

Table 2 presents the bulk density results measured across five cross-sections of the LAAM cylinders at one day after casting. For all mixtures, the differences in unit weight among sections were relatively small, indicating that no significant segregation occurred during casting and early curing. The reference mixture without UCG (LC-00 mixture) showed an average bulk density of 1630 kg/m^3 with a standard deviation of 45.8 kg/m^3. The mixtures incorporating UCG at 5 % (LC-05 mix) and 10 % (LC-10 mix) exhibited comparable average densities of 1644 and 1516 kg/m^3, with lower standard deviations of 24.5 and 25.8 kg/m^3, respectively. These reduced variations suggest that the partial replacement of BA with UCG did not negatively affect the homogeneity of the mixture. The LC-15 mixture, containing the highest UCG content, showed the lowest average density (1401 kg/m^3) and a slightly larger standard deviation (42.4 kg/m^3). Although the variation increased relative to LC-05 and LC-10, the magnitude remained within an acceptable range and did not indicate notable stratification. The moderate fluctuation may be attributed to the lower density and higher porosity of UCG, which could influence particle distribution during mixing. Overall, the results suggest that UCG replacements up to 15% by volume do not lead to considerable segregation. This finding confirms the suitability of UCG as a fine lightweight aggregate in LAAM mixtures, ensuring uniformity and structural integrity at early ages.

Table 2. The difference in bulk density between different cross-sections of the LAAM.

Sections	LC-00	LC-05	LC-10	LC-15
S1	1638	1675	1528	1340
S2	1656	1638	1524	1421
S3	1643	1649	1528	1388
S4	1662	1608	1471	1401
S5	1550	1649	1532	1454
Average	1630	1644	1516	1401
Standard deviation	*45.8*	*24.5*	*25.8*	*42.4*

According to BS EN 206-1 classification criteria, structural lightweight concrete/ mortar typically exhibits oven-dry densities below approximately 2000 kg/m^3 [27]. Thus, it could be observed that the measured densities of all LAAM mixtures clearly fall within the lightweight range.

3.2. Compressive strength

Figure 3 shows the compressive strength results of LAAM mixtures at 7, 28, and 56 days. In general, the incorporation of UCG led to a noticeable reduction in strength compared with the reference mix, except for LC-05, which exhibited a slight improvement. The control mixture (LC-00) reached strengths of 30.7, 34.2, and 35.2 MPa at 7, 28, and 56 days, respectively. The LC-05 mixture demonstrated the highest strength among all mixes, recording 31.8 MPa at 7 days and increasing to 40.1 MPa at 56 days, representing an improvement of approximately 14 % compared with LC-00. This enhancement may be attributed to the microstructural continuity enhancement at low replacement levels, possibly due to localized pore refinement and moderated moisture redistribution and improved particle packing arising from the small dosage of UCG, which likely contributed to a denser matrix. In addition, the porous structure of UCG at low replacement levels may act as an internal curing reservoir, supplying additional moisture to promote continued alkali-activation reactions and gel formation, thereby contributing to a more continuous and compact matrix. However, when the UCG content exceeds this optimal level, the negative effects associated with increased void volume and

weaker interfacial bonding dominate, leading to a reduction in compressive strength. This optimum-type response reflects a balance between localized densification and internal moisture buffering at low UCG dosage and the progressive formation of a defect-rich load-transfer skeleton at higher replacement levels. Within this framework, compressive strength is governed primarily by matrix continuity and effective stress-transfer pathways rather than total porosity alone, explaining the initial enhancement at 5 % UCG and subsequent deterioration at higher contents.

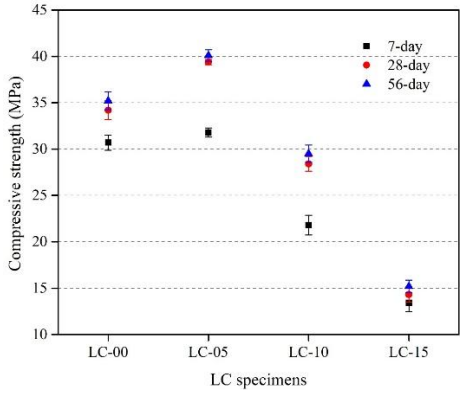

Figure 3. Compressive strength of LAAM.

In contrast, higher UCG replacement levels (LC-10 and LC-15) resulted in significant strength reductions, consistent with findings from previous research [11]. The LC-10 mixture reached strengths of 21.8, 28.4, and 29.5 MPa at 7, 28, and 56 days, while LC-15 showed the lowest strengths at each age (13.4, 14.3, and 15.2 MPa). The reduction in strength is likely associated with the increased porosity and reduced mechanical rigidity resulting from greater UCG incorporation [12]. Although strength development over time was observed for all mixtures, the growth rate diminished at higher UCG contents, indicating that excessive replacement weakens the structural integrity of the LAAM matrix. Based on the National standard classification [28], the LC-00 and LC-05 correspond to grade M30, the LC-10 corresponds to grade M20, and the LC-15 corresponds to grade M10. These findings suggest that UCG has a threshold level for beneficial inclusion. A low replacement level (5 %) can enhance compressive strength, while higher incorporation levels adversely affect mechanical performance.

3.3. Ultrasonic pulse velocity

Figure 4 shows the UPV results of LAAM specimens at 7, 28, and 56 days. A general increase in UPV was observed over time for all mixtures, reflecting continued matrix densification and microstructural development. The LC-05 mixture consistently exhibited the highest UPV values, reaching 3498, 3586, and 3631 m/s at 7, 28, and 56 days, respectively. These values surpassed those of the control mix (LC-00), which recorded 3341–3429 m/s across the same ages. The higher UPV in LC-05 indicates improved structural compactness and better transmission of ultrasonic waves, likely due to enhanced particle packing and effective integration of UCG at low replacement levels. Conversely, increasing UCG content beyond 5 % resulted in progressively lower UPV values. LC-10 showed moderately reduced UPV (3284–3311 m/s), while LC-15 demonstrated the lowest values, ranging from 3064 to 3218 m/s. These reductions imply greater internal defects and porosity at higher UCG dosages, which impede wave propagation and weaken the matrix. Despite this, UPV increased slightly with curing age for LC-10 and LC-15, suggesting continued but limited geopolymerization. According to Solís-Carcaño and Moreno [29], UPV quality classifications were originally proposed for normal-weight concrete. Since LAAM possesses lower density and inherently higher porosity than conventional concrete, direct application of these thresholds may lead to conservative classification. Therefore, the referenced criteria are used herein solely for comparative interpretation, rather than as a definitive quality grading framework for LAAM. It should be noted that UPV values in lightweight and alkali-activated systems are strongly influenced by density, pore connectivity, and impedance mismatch between aggregate and binder phases; consequently, direct comparison with normal-weight concrete benchmarks should be interpreted with caution. Overall, the UPV results align well with the compressive strength trends, confirming that a 5 % UCG replacement enhances matrix integrity, while higher contents adversely affect the internal structure and wave propagation characteristics of LAAM.

The correlation between compressive strength and UPV is expressed by a linear relationship, as shown in Figure 5. The regression incorporates all experimental data points obtained from four mixtures (LC-00, LC-05, LC-10, and LC-15) at curing ages of 7, 28, and 56 days. The resulting relationship therefore reflects a compressive strength interval of approximately 13–40 MPa and a corresponding UPV range of approximately 3060–3630 m/s within the investigated FA–GGBFS LAAM system. Because the obtained correlation is mixture-specific and continuity-controlled, it can only be applied to the studied density range and binder system; extrapolation outside of this range should be done with caution. As the compressive strength increases from approximately 14 to 40 MPa, the UPV values rise correspondingly from about 3050 to over 3600 m/s. This trend indicates a progressive densification of the material matrix, associated with reduced porosity and improved internal continuity. The linear regression analysis yields a high coefficient of determination ($R^2 \approx 0.84$), confirming a strong and reliable correlation between the two parameters. The slope of the regression line ($\approx$ 16.2 m/s per MPa) suggests that UPV is sensitive to changes in compressive strength. These results support the applicability of UPV as an effective non-destructive indicator for assessing the mechanical quality and overall integrity of LAAM. It should be emphasized that UPV is interpreted herein as an indicator of internal continuity and defect population, which are structurally relevant to long-term performance, but it does not substitute for direct durability testing under aggressive

environmental exposures. In the present system, UPV is interpreted as a continuity-sensitive parameter that reflects internal defect population and pore connectivity. The strong linear correlation between compressive strength and UPV ($R^2 \approx 0.84$) confirms that matrix continuity governs both wave propagation and load-bearing capacity within the investigated UCG replacement range. It should be noted that this empirical relationship is mixture-specific and valid within the investigated range of LAAM; therefore, extrapolation beyond the studied material system should be approached with caution.

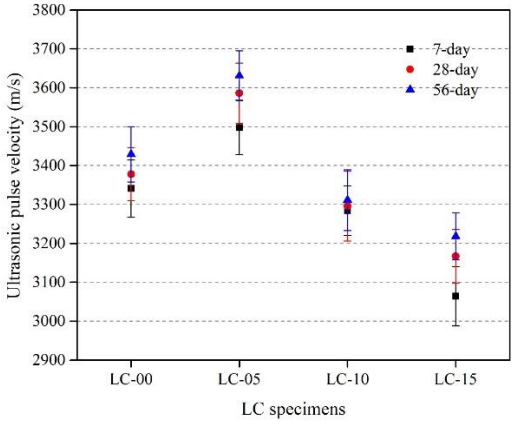

Figure 4. UPV of LAAM.

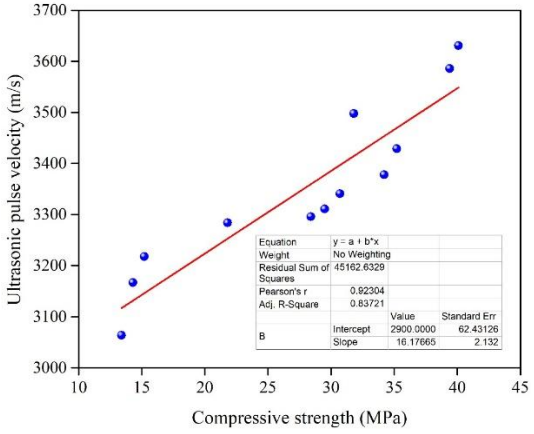

Figure 5. Correlation between compressive strength and UPV of LAAM.

3.4. Drying shrinkage

The drying shrinkage results of the LAAM specimens are presented in Figure 6. All mixtures exhibited a progressive increase in shrinkage with curing age, stabilizing after 28 days. The control mix (LC-00) demonstrated the highest shrinkage, reaching −308.3 μm/m at 56 days, indicating substantial volumetric contraction due to moisture loss and matrix densification. In contrast, the incorporation of UCG effectively reduced drying shrinkage across all ages. At 56 days, LC-05, LC-10, and LC-15 recorded shrinkage values of −138.5, −183.9, and −124.8 μm/m, reductions of approximately 55 %, 40 %, and 60 % compared with LC-00, respectively. The reduced shrinkage is likely attributed to the highly porous nature and water-retention capability of UCG, which facilitates internal curing and helps mitigate stress development within the matrix. In addition to internal moisture buffering, the increased compliance introduced by porous UCG particles may reduce shrinkage-induced stress despite higher overall porosity. This dual contribution helps explain the non-linear relationship between shrinkage and compressive strength at higher UCG replacement levels. Among the modified mixtures, LC-15 exhibited the lowest shrinkage throughout the curing period, suggesting that higher UCG contents improve dimensional stability. However, LC-10 showed slightly higher shrinkage than LC-05 and LC-15, implying that shrinkage behavior may not be linearly correlated with UCG content. The non-linear shrinkage evolution arises from the interaction of three competing mechanisms: (i) internal moisture buffering provided by pre-saturated porous UCG particles, which mitigates capillary stress development; (ii) increased pore connectivity at intermediate replacement levels, which facilitates moisture transport and strain development; and (iii) reduced composite stiffness at higher UCG contents, which lowers restraint stress and therefore decreases measured shrinkage strain despite higher total porosity. Consequently, shrinkage in this system is governed by a moisture–continuity–compliance coupling rather than by porosity alone. This explains why LC-15 exhibits lower shrinkage than LC-10 even though its compressive strength is lower. The results confirm that the addition of UCG significantly decreases drying shrinkage, highlighting its beneficial role in enhancing the dimensional stability of LAAM. Within the continuity-controlled framework proposed in this study, dimensional stability reflects the combined effects of moisture redistribution, pore connectivity, and matrix stiffness, rather than a direct function of strength or density alone. The inverse relationship observed between shrinkage reduction and compressive strength at higher UCG contents reflects a classical stiffness–compliance trade-off commonly observed in porous composite systems.

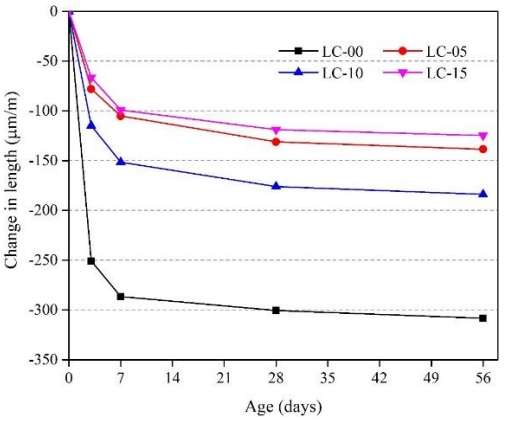

Figure 6. Length change in the LAAM samples.

3.5. Microstructure analysis

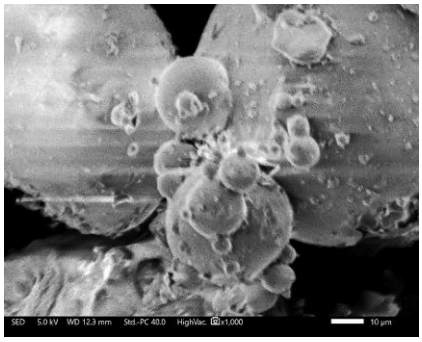

(a) BA

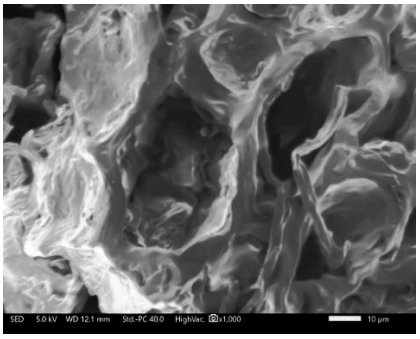

(b) UCG

Figure 7. SEM images of BA and UCG.

The SEM observations (Figure 7) clearly highlight the distinct morphological characteristics of BA and UCG particles and their implications for LAAM's performance. The BA particles exhibit a predominantly spherical to sub-spherical morphology with relatively smooth surfaces and fly ash–like characteristics; as a fine aggregate, this morphology is beneficial for particle packing and interfacial contact. It can also contribute to improved workability and a denser microstructure through the ball-bearing effect. In contrast, the UCG particles show a highly irregular and porous structure with large, interconnected internal voids. Such pronounced porosity significantly increases water absorption and reduces the effective load-bearing area within the composite matrix. Similar trends have been reported in cementitious mortars incorporating porous bio-derived fillers eased internal porosity and reduce effective load-transfer area, commonly leading to mechanical reductions, even when moisture-buffering or functional benefits are obtained. Furthermore, coffee-waste-derived additions have been shown to affect matrix development depending on processing route, with porosity and interfacial quality governing the net strength response [30], [31]. As a result, UCG acts more as a lightweight filler than a structural aggregate, which explains its strong influence on density reduction and mechanical performance. The clear microstructural contrast between BA and UCG observed in the SEM images provides direct evidence linking particle morphology and internal porosity to the physical and mechanical behavior of the lightweight composites investigated in this study.

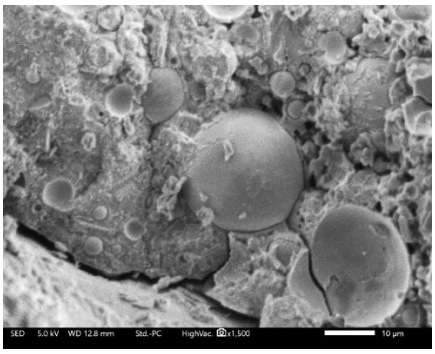

(a) LC-00

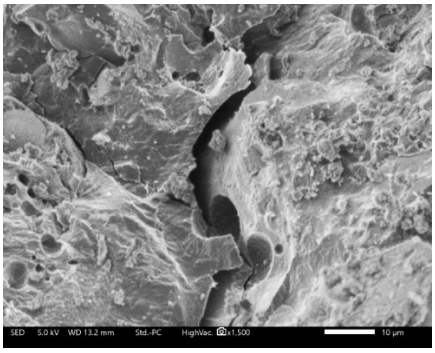

(b) LC-05

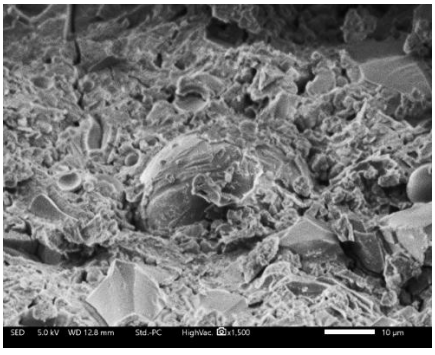

(c) LC-10

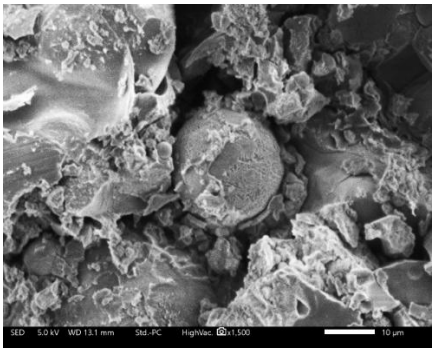

(d) LC-15

Figure 8. SEM micrographs of LAAM.

The SEM micrographs of the LAAM mixtures are shown in Figure 8. In LC-05 (Figure 8b), good interfacial contact between BA and UCG is observed, and most particles are well embedded within the

geopolymer matrix, resulting in minimal visible voids. This dense microstructure explains why LC-05 achieved the highest compressive strength and UPV among all mixtures. In contrast, the other mixtures display several unembedded BA particles and a rougher, more porous surface. This effect becomes particularly evident in LC-15, where the extensive porosity suggests a less compact matrix and weaker particle–paste bonding. The increased connectivity of voids and the presence of porous interfacial transition zones around UCG particles reduce the effective load-transfer area and hinder ultrasonic wave propagation, which explains the observed reductions in compressive strength and UPV. At the same time, the porous UCG particles act as internal moisture reservoirs, contributing to the reduced drying shrinkage observed in mixtures with higher UCG contents. These microstructural observations are consistent with the mechanical and durability results discussed previously.

Overall, the SEM results provide a unifying explanation for the macroscopic trends observed in this study. Mixtures with a more continuous gel network and fewer connected voids enable more effective stress transfer under compression and reduce wave scattering during UPV testing, leading to higher compressive strength and UPV. Conversely, the presence of connected pores and discontinuities weakens the load-bearing skeleton and disrupts ultrasonic transmission, which is consistent with the reductions in both properties at higher UCG contents. Importantly, the acceptable uniformity observed in the segregation test indicates that these performance changes are primarily governed by microstructural evolution rather than density stratification, reinforcing the microstructure–property link in LAAM mixtures. The denser matrix and improved particle–paste interlocking in LC-05 correspond well with its superior compressive strength and highest UPV values, confirming that enhanced gel formation and reduced internal defects contribute to more efficient stress-wave transmission and mechanical load resistance. Conversely, LC-10 and LC-15 exhibit increasingly porous microstructures, which align with their lower compressive strength and reduced UPV measurements. The greater presence of voids and weak interfacial zones in these mixtures likely provides pathways for crack propagation, resulting in diminished structural integrity.

4. Conclusions

This study investigated the influence of used coffee grounds (UCG) as a partial fine aggregate replacement on the properties of LAAM. The key findings are summarized as follows:

- All mixtures showed satisfactory uniformity, with minor variations in bulk density, indicating that UCG incorporation up to 15 % did not cause noticeable segregation.

- Incorporating 5 % UCG enhanced compressive strength and achieved the highest UPV, reflecting an optimal balance between particle packing and internal curing. However, further increases in UCG content progressively reduced both strength and UPV, as the adverse effects of increased porosity and weaker particle–matrix bonding became dominant.

- UCG-modified mixtures generally exhibited lower drying shrinkage than the control mixture. Among them, LC-15 consistently showed the lowest shrinkage, while LC-10 exhibited slightly higher values than LC-05 and LC-15, indicating that shrinkage behavior does not vary linearly with UCG content. This reduction is primarily attributed to the internal curing effect provided by the highly porous UCG particles.

- SEM results confirmed superior matrix compactness in LC-05, with effective embedding of BA and UCG in the geopolymer gel. Higher UCG levels led to more voids and poorer interfacial contact, consistent with declines in mechanical and UPV performance.

- The test results indicate that a UCG content of approximately 5 % provides the best overall performance, making it the most suitable level for practical application.

Overall, the combined strength–UPV–shrinkage trends and SEM observations consistently indicate that matrix continuity and pore/ITZ characteristics govern the macroscopic behavior of UCG-modified LAAM. The mechanism proposed herein is therefore continuity-based rather than chemically resolved at the phase assemblage level. Denser gel networks with fewer connected voids, as observed in LC-05, facilitate more effective stress transfer and ultrasonic wave propagation, while also limiting moisture loss during drying. In contrast, the increased pore connectivity and interfacial discontinuities at higher UCG contents explain the simultaneous reductions in strength and UPV, despite improvements in shrinkage behavior. It should be noted that the present study evaluates dimensional stability and structural integrity indicators rather than exposure-based durability performance. Further investigations involving chloride penetration, sulfate attack, freeze–thaw resistance, and long-term environmental exposure are necessary to comprehensively assess the durability of UCG-based LAAM.

Acknowledgment

The authors gratefully acknowledge the Huynh's Research Group at Can Tho University for their valuable support and assistance throughout the experimental program.

References

[1]. S.-H. Ngo and T.-P. Huynh, "Effect of paste content on long-term strength and durability performance of green mortars," *Journal of Science and Technology in Civil Engineering*, vol. 16, no. 1, pp. 113–125, 2022, doi: 10.31814/stce.huce(nuce)2022-16(1)-10.

[2]. C. Nab and M. Maslin, "Life cycle assessment synthesis of the carbon footprint of Arabica coffee: Case study of Brazil and Vietnam conventional and sustainable coffee production and export to the United Kingdom," *Geo: Geography and Environment*, vol. 7, no. 2, p. e00096, 2020, doi: 10.1002/geo2.96.

[3]. X. C. Schmidt Rivera, A. Gallego-Schmid, V. Najdanovic-Visak, and A. Azapagic, "Life cycle environmental sustainability of valorisation routes for spent coffee grounds: From waste to resources," *Resources, Conservation and Recycling*, vol. 157, p. 104751, 2020, doi: 10.1016/j.resconrec.2020.104751.

[4]. D. Eliche-Quesada *et al.*, "The use of different forms of waste in the manufacture of ceramic bricks," *Applied Clay Science*, vol. 52, no. 3, pp. 270–276, 2011, doi: 10.1016/j.clay.2011.03.003.

[5]. F. Andreola *et al.*, "Spent coffee grounds in the production of lightweight clay ceramic aggregates in view of urban and agricultural sustainable development," *Materials*, vol. 12, pp. 3581, 2019, doi: 10.3390/ma12213581.

[6]. L. L. P. Chung, Y. C. Wong, and A. Arulrajah, "The application of spent coffee grounds and tea wastes as additives in alkali-activated bricks," *Waste and Biomass* Valorization, vol. 12, no. 11, pp. 6273–6291, 2021, doi: 10.1007/S12649-021-01453-7.

[7]. S. Na, S. Lee, and S. Youn, "Experiment on activated carbon manufactured from waste coffee grounds on the compressive strength of cement mortars," *Symmetry*, vol. 13, no. 4, 2021, doi: 10.3390/sym13040619.

[8]. D. Eliche-Quesada, L. Pérez-Villarejo, F. J. Iglesias-Godino, C. Martínez-García, and F. A. Corpas-Iglesias, "Incorporation of coffee grounds into clay brick production," *Advances in Applied Ceramics*, vol. 110, no. 4, pp. 225–232, 2011, doi: 10.1179/1743676111Y.0000000006.

[9]. A. Lachheb *et al.*, "Thermal insulation improvement in construction materials by adding spent coffee grounds: An experimental and simulation study," *Journal of Cleaner Production*, vol. 209, pp. 1411–1419, 2019, doi: 10.1016/j.jclepro.2018.11.140.

[10]. R. Roychand, S. Kilmartin-Lynch, M. Saberian, J. Li, G. Zhang, and C. Q. Li, "Transforming spent coffee grounds into a valuable resource for the enhancement of concrete strength," *Journal of Cleaner Production*, vol. 419, no. 2023, doi: 10.1016/j.jclepro.2023.138205.

[11]. J. Lee, J. Kim, and S. Lee, "Study of recycled spent coffee grounds as aggregates in cementitious materials," *Recent Progress in Materials*, vol. 05, no. 01, pp. 1–23, 2023, doi: 10.21926/RPM.2301007.

[12]. M. Guendouz, D. Boukhelkhal, Z. Triki, A. Mechantel, and T. Boukerma, "Effect of using spent coffee grounds wastes as aggregates on physical and thermal properties of sand concrete," *Algerian Journal of Environmental Science*, vol. 9, pp. 3256–3264, 2023.

[13]. B. Y. Yun, H. M. Cho, Y. U. Kim, S. C. Lee, U. Berardi, and S. Kim, "Circular reutilization of coffee waste for sound absorbing panels: A perspective on material recycling," *Environmental Research*, vol. 184, p. 109281, 2020, doi: https://doi.org/10.1016/j.envres.2020.109281.

[14]. T. Moussa *et al.*, "Spent coffee grounds as building material for non-load-bearing structures," *Materials*, vol. 15, no. 5, 2022, doi: 10.3390/ma15051689.

[15]. C. Liu, Z. Li, and G. Ye, "Mitigating the efflorescence of alkali-activated slag mortars by aluminosilicate-based lightweight fine aggregate," *Cement and Concrete Research*, vol. 195, p. 107917, 2025, doi: 10.1016/j.cemconres.2025.107917.

[16]. E. Vasanelli, S. Calò, A. Cascardi, and M. A. Aiello, "The use of lightweight aggregates in geopolymeric mortars: the effect of liquid absorption on the physical/mechanical properties of the mortar," *Materials*, vol. 17, no. 8, p. 1798, 2024, doi: 10.3390/ma17081798.

[17]. D. P. Bentz, "Influence of internal curing using lightweight aggregates on interfacial transition zone percolation and chloride ingress in mortars," *Cement and Concrete Composites*, vol. 31, no. 5, pp. 285–289, 2009, doi: 10.1016/j.cemconcomp.2009.03.001.

[18]. W. Shen, L. Wang, P. Chen, H. Wang, and K. Cao, "Mitigating autogenous shrinkage of alkali-activated slag mortar by using porous fine aggregates as internal curing agents," *Sustainability*, vol. 14, no. 16, p. 9823, 2022, doi: 10.3390/su14169823.

[19]. T. H. Y. Nguyen, N. T. Cao, T. D. M. Ngoc, and T. P. Huynh, "Experimental evaluation on engineering properties and drying shrinkage of no-cement mortar produced by alkaline activation of fly ash-slag mixtures," *Engineering Journal*, vol. 26, no. 3, pp. 17–28, 2022, doi: 10.4186/ej.2022.26.3.17.

[20]. ASTM C1437-20, "*Standard test method for flow of hydraulic-cement mortars*." ASTM International, West Conshohocken, PA, USA, 2020.

[21]. N. C. Thang *et al.*, "Experimental study to produce lightweight concrete using recycled expanded Polystyrene," *Journal of Science and Technology in Civil Engineering*, vol. 15, no. 1V, pp. 72–83, 2021, doi: 10.31814/stce.nuce2021-15(1V)-07.

[22]. A. Miguel Solak, A. José Tenza-Abril, and V. Eugenia García-Vera, "Adopting an image analysis method to study the influence of segregation on the compressive strength of lightweight aggregate concretes," *Construction and Building Materials*, vol. 323, p. 126594, 2022, doi: 10.1016/j.conbuildmat.2022.126594.

[23]. F. S. Barbosa, A.-L. Beaucour, M. C. R. Farage, and S. Ortola, "Image processing applied to the analysis of segregation in lightweight aggregate concretes," *Construction and Building Materials*, vol. 25, no. 8, pp. 3375–3381, 2011, doi: 10.1016/j.conbuildmat.2011.03.028.

[24]. ASTM C349-18, "*Standard test method for compressive strength of hydraulic-cement mortars (using portions of prisms broken in flexure)*." ASTM International, West Conshohocken, PA, USA, 2018.

[25]. ASTM C597-22, "*Ultrasonic pulse velocity through concrete*," ASTM International, West Conshohocken, PA, USA, 2022.

[26]. ASTM C490/C490M-21, "*Standard practice for use of apparatus for the determination of length change of hardened cement paste, mortar, and concrete*," ASTM International, West Conshohocken, PA, USA, 2021.

[27]. L. Prasittisopin, P. Termkhajornkit, and Y. H. Kim, "Review of concrete with expanded polystyrene (EPS): Performance and environmental aspects," *Journal of Cleaner Production*, vol. 366, p. 132919, 2022, doi: 10.1016/j.jclepro.2022.132919.

[28]. TCVN 4314:2022, "*Mortar for masonry - Specifications*," Ministry of Science and Technology, Ha Noi, Viet Nam, 2022. (in Vietnamese).

[29]. R. Solís-Carcaño and E. I. Moreno, "Evaluation of concrete made with crushed limestone aggregate based on ultrasonic pulse velocity," *Construction and Building Materials*, vol. 22, no. 6, pp. 1225–1231, 2008, doi: 10.1016/j.conbuildmat.2007.01.014.

[30]. R. Mrad and G. Chehab, "Mechanical and microstructure properties of biochar-based mortar: an internal curing agent for PCC," *Sustainability*, vol. 11, no. 9, p. 2491, 2019, doi: 10.3390/su11092491.

[31]. R. Roychand, S. Kilmartin-Lynch, M. Saberian, J. Li, G. Zhang, and C. Q. Li, "Transforming spent coffee grounds into a valuable resource for the enhancement of concrete strength," *Journal of Cleaner Production*, vol. 419, p. 138205, 2023, doi: 10.1016/j.jclepro.2023.138205.